

Pseudo-label Guided Cross-video Pixel Contrast for Robotic Surgical Scene Segmentation with Limited Annotations

Yang Yu, Zixu Zhao, Yueming Jin, Guangyong Chen, Qi Dou and Pheng-Ann Heng

Abstract—Surgical scene segmentation is fundamentally crucial for prompting cognitive assistance in robotic surgery. However, pixel-wise annotating surgical video in a frame-by-frame manner is expensive and time consuming. To greatly reduce the labeling burden, in this work, we study semi-supervised scene segmentation from robotic surgical video, which is practically essential yet rarely explored before. We consider a clinically suitable annotation situation under the equidistant sampling. We then propose *PGV-CL*, a novel pseudo-label guided cross-video contrast learning method to boost scene segmentation. It effectively leverages unlabeled data for a trusty and global model regularization that produces more discriminative feature representation. Concretely, for trusty representation learning, we propose to incorporate pseudo labels to instruct the pair selection, obtaining more reliable representation pairs for pixel contrast. Moreover, we expand the representation learning space from previous image-level to cross-video, which can capture the global semantics to benefit the learning process. We extensively evaluate our method on a public robotic surgery dataset EndoVis18 and a public cataract dataset CaDIS. Experimental results demonstrate the effectiveness of our method, consistently outperforming the state-of-the-art semi-supervised methods under different labeling ratios, and even surpassing fully supervised training on EndoVis18 with 10.1% labeling. Our code is available at <https://github.com/yangyu-cuhk/PGV-CL>.

Index Terms—Scene segmentation, pixel-level contrastive learning, semi-supervised learning, robotic surgical video

I. INTRODUCTION

With the assistance of medical robot, minimally invasive surgery (MIS) has greatly reshaped patient care, bringing safer surgery procedure and shorter recovery time [1]. Semantic scene segmentation from surgical video is an essential prerequisite for robot-assisted system. By providing pixel-wise context of instrument and anatomy, it can facilitate cognitive assistance, serving as a building block for higher-level perception, such as surgical decision making [2] and skill assessment [3]. In addition, whole scene mask can help selectively render different parts in the augmented reality environment, bringing new possibilities for robotic surgery education and navigation [4]. Precise identifying the robotic

This work was supported by Key-Area Research and Development Program of Guangdong Province, China under Grant 2020B010165004, Hong Kong RGC TRS Project No. T42-409/18-R and Hong Kong Innovation and Technology Fund Project No. GHP/080/20SZ.

Y. Yu, Z. Zhao, Q. Dou and P. A. Heng are with the Department of Computer Science and Engineering, The Chinese University of Hong Kong, Hong Kong. P. A. Heng is also with Guangdong Provincial Key Laboratory of Computer Vision and Virtual Reality Technology, Shenzhen Institutes of Advanced Technology, Chinese Academy of Sciences, Shenzhen, China. Yueming Jin is with the Wellcome/EPSCRC Centre for Interventional and Surgical Sciences (WEISS) and the Department of Computer Science, University College London. G. Chen is with Zhejiang Lab.

Corresponding author: Yueming Jin (yueming.jin@ucl.ac.uk)

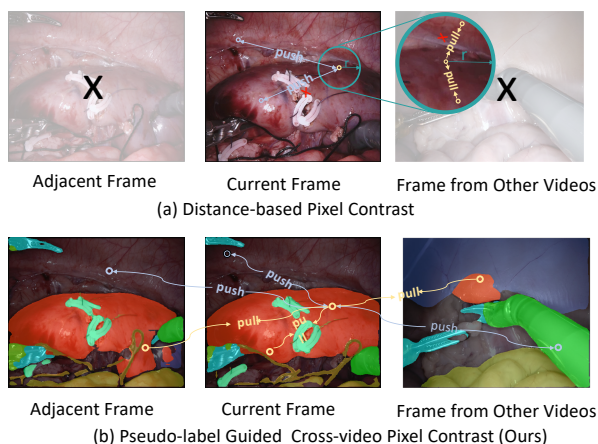


Fig. 1. (a) Distance-based pixel contrast can only utilize current frame and pulls (pushes) representations of pixel pair nearby (faraway). (b) Our method leverages *pseudo labels* as guidance for trusty contrast, pulling (pushing) representations of pixel pair belonging to the same (different) class. Our pixel pairs are selected *cross-video* to conduct global contrast.

instruments is also a critical technique for tool pose estimation [5], robot control [6] and surgical task automation [7].

Recently, convolutional neural networks have achieved remarkable successes in surgical scene segmentation [4], [8]–[11] given large amounts of labeled data. For example, Ren et al. [8] decompose the task into different levels and coordinate multi-task learning. However, it is time consuming and laborious for experienced surgeons to perform dense pixel-wise frame-by-frame annotations. In this work, we study semi-supervised scene segmentation by utilizing scarce labeled data and abundant unlabeled data, which is a highly desired task for practical usage yet still underexplored in the robotic surgery scenario. Meanwhile, it is highly challenging to precisely segment both tool and anatomy in the complicated surgical scene, given the low inter-class variation between tissues, extremely tiny size of some objects such as thread, and inevitable visual occlusion from blood, tool motion blurriness, and lighting changes.

Two main streams of approaches have been proposed for semi-supervised semantic segmentation, however, we identify the corresponding limitations of each stream when tackling the surgical scene segmentation with few annotations. The first stream is generating pseudo labels for unlabeled data by employing the model trained on labeled data, e.g., using segmentation model predictions [12], [13], or using motion flow to propagate pseudo labels [14], [15]. Recent studies are dedicated to improving the quality, e.g., utilizing model confidence to filter out poor labels [16]–

[18], or developing several models and leveraging the inter-model disagreement to locate label errors [19]. Even though undergoing the error filtering, all these methods explicitly regard pseudo labels as ground truth to calculate loss for model penalization at the end. It is sub-optimal for analyzing highly complex robotic surgical scene, as the inevitable noise in pseudo labels degrades the model training when using this explicit supervision (see Sec. III-C). How to more effectively leverage the pseudo label for surgical scene segmentation is still an open question to be solved.

Recent advances are dedicated to the other direction, which aims to extract knowledge from unlabeled data through self-supervised regularization. Consistency regularization methods [20]–[22] are first proposed to regularize the model to produce consistent predictions when inputting an unlabeled data with different perturbations. Contrastive learning emerges to regularize the model in a higher-level feature space [23], [24]. The core idea is to attract similar (positive) and repulse dissimilar (negative) pairs of features extracted from unlabeled data, to provide a good model initialization. With advanced representation capability, after using limited labeled data for fine-tuning, the model can achieve precise scene segmentation [25], [26]. One main investigation direction is how to accurately construct the positive and negative pairs, given its key role in contrastive learning [23]–[25], [27]. Some methods construct pairs based on the pixel location [25]–[27]. For example, Xie et al. [27] utilize the spatial distance with the assumption that neighborhood pixels generally belong to the same class and can form the positives. However, extensive exceptions will appear in the robotic surgical scene. See Fig. 1(a), different tissues and instruments with irregular shape generally present at the same time, bringing massive class boundaries. Pixels near these boundaries are hardly formed to be the precise pairs. Moreover, most existing methods construct pairs purely from the current single image, ignoring the valuable sequential information in robotic surgical video.

In this work, we propose a novel **pseudo-label guided cross video contrast learning (PGV-CL)**, to tackle semi-supervised scene segmentation of robotic surgical video. Our contrastive paradigm can boost the segmentation performance via a *trusty* and *global* regularization. It enhances the model representation learning from two perspectives, i.e., the accuracy and adequacy of the contrast representation space. Specifically, we first devise an equidistant sampling strategy for semi-supervised scene segmentation, i.e., only performing the labeling at interval, to maximize the quality of pseudo labels. Unlike previous methods treating pseudo labels as ground truth for explicit model regularization by loss, we propose to use the pseudo labels as the guidance for pair construction in contrastive learning, sharing the same spirit with very recent works that devise a label-based contrastive loss [28]–[30]. Our implicit way to use the pseudo label bypasses accumulating mistakes when treating it as ground truth, and can greatly increase the preciseness in contrastive training. Moreover, it enables to borrow more knowledge in robotic surgical videos in contrastive training. Here, we

consider two properties: i) robotic surgical video presents the inherent sequential nature of robotic surgical video, where adjacent frames share the similarity semantic information; ii) different surgical procedures generally present various appearances due to different lighting conditions, patient cohorts, or surgeon operative skills. In combination with the pseudo label guidance, we propose a cross-video pixel contrast, introducing the more aggressive positive pairs from the adjacent frames, and natural negative pairs from different videos, to enlarge the contrast space.

With the increase in both accuracy and adequacy for contrast, our method can shape a better structure in the global representation space, and providing better model initialization. To this end, only using extreme limited annotations, our method can achieve accurate segmentation on surgical scene. Our main contributions are summarized as follows:

- We take the first step to integrate the pseudo label into contrastive learning for semi-supervised scene segmentation of robotic surgical video, contributing to the accurate and trusty pixel contrast with guidance.
- We develop a novel four-level hierarchical pair construction for cross-video contrast, which leverages the inherent properties of robotic surgical videos, to consider the global semantics of the whole dataset in feature representation learning.
- We extensively validate our method on a public robotic surgery dataset EndoVis18 [4] and a public cataract dataset CaDIS [9]. Our method consistently outperforms state-of-the-art semi-supervised methods by a large margin, even exceeding the fully supervised training with 10.1% labels on EndoVis18.

II. METHODS

Fig. 2 presents the overview of proposed PGV-CL for semi-supervised scene segmentation from robotic surgical video. We first describe the problem setting with devised annotation sampling strategy, which can also provides relatively accurate pseudo labels. We then introduce our pseudo-label guided mechanism and cross-video pair construction to better shape the pixel representation space, from two aspects of the accuracy and adequacy of contrast.

A. Equidistant Sampling for Semi-supervised Segmentation

Adjacent frames from the surgical video generally share the similar appearance, making model easily parse the scene after seeing one of them. To maximize the quality of pseudo label under the same annotation efforts, we propose an equidistant sampling strategy, where the annotation is performed sparsely on each training video sequence with an interval. Given a video having T frames as $V = \{x_0, x_1, \dots, x_{T-1}\}$, we assume that only $\{x_0, x_{1 \times h}, \dots, x_{t \times h}\}$ are labeled with interval h , where $t \times h$ is the largest integer smaller than $T - 1$. For example, annotating the surgical video with the interval 9 accounts for 10% labeled data. With equidistant sampling strategy, our model generates relatively accurate pseudo label for unlabeled frames, as shown in Fig. 7. And the pseudo label is accurate enough, thus it is

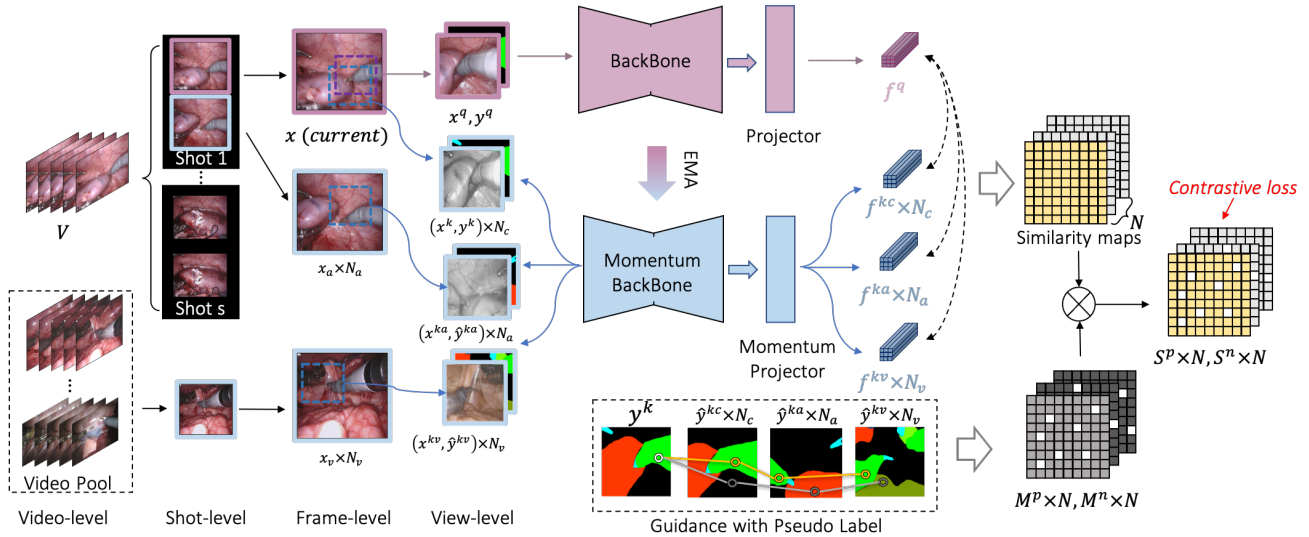


Fig. 2. Overview of proposed PGV-CL. It goes through the four-level hierarchy to form the cross-video query x^q and key $\{x^k, x^{ka}, x^{kv}\}$ image samples as the input of model. Dense query and key feature maps are respectively generated by two symmetric branches of the model, for calculating the similarity between per pixel, obtaining one similarity map for each query-key image pair. We then exploit corresponding pseudo labels as the guidance to pair query and key pixels to positive \mathcal{M}^p and negative \mathcal{M}^n ones. Based on these, similarities can be partitioned to S^p and S^n for the pixel-wise contrastive learning.

directly used to guide our cross-video pixel contrast. This setting is also favorable to clinical practice, as it is easier for surgeons to perform low hertz labeling of surgical video.

With the interval h , the whole dataset consists of labeled subset $\mathcal{D}_L = \{(x_t, y_t)\}_{t=hn}$ and unlabeled subset $\mathcal{D}_U = \{x_t\}_{t \neq hn}$. We first train a segmentation model $\mathcal{F}^s : \{x_t\} \rightarrow \{y_t\}$ using the labeled subset, and use f^s to generate the pseudo labels, obtaining $\hat{\mathcal{D}}_U = \{x_t, \hat{y}_t\}_{t \neq hn}$. $\hat{\mathcal{D}}_U$ is then utilized for the pseudo label guided contrastive learning.

B. Pseudo-label Guided Contrast for Trusty Regularization

Contrastive learning can enhance the discriminative capability of the model by self-training on unlabeled data. Given an image $x \in \mathbb{R}^{H \times W \times 3}$ as the query sample and a set of images as key samples, image-level contrastive learning train the model \mathcal{F}^{CL} by distinguishing the positives (augmentation version of x) from negatives (from training set excluding x). The contrastive loss is based on the similarity principle between the feature embeddings of these data samples: $f = \mathcal{F}^{CL}(x)$, $f \in \mathbb{R}^D$, D is the feature channel.

For the dense surgical scene segmentation, we explore a pixel-level contrastive learning by extending data sample from image to image pixel. Concretely, we perform different augmentations on the current frame x and generate two views x^q as query and x^k as key. With two symmetric branches of our framework (cf. Fig. 2), x^q is fed into a regular encoder branch to predict the query feature map: $f^q = \mathcal{F}_q^{CL}(x^q)$, and likewise, x^k is fed into a momentum encoder branch to predict the key feature map: $f^k = \mathcal{F}_k^{CL}(x^k)$. The encoder branches are composed of a backbone model and a projection head. We employ our pre-trained segmentation model \mathcal{F}^s without classifier as the backbone, to well-initialize most layers. Directly applying the contrastive objective onto the features would regularize the representation learning too heavily, we thus construct a projection head to map the

features to a lower-dimension space. With the feature maps $f^q, f^k \in \mathbb{R}^{H \times W \times D}$, we can extract the pixel-level feature embeddings, denoting the query embedding as f_i^q and the key embedding as f_j^k for the i and j pixel, respectively. We then compute the cosine distance on the obtained embeddings:

$$S_{ij} = \frac{\langle f_i^q, f_j^k \rangle}{\|f_i^q\| \|f_j^k\|}. \quad (1)$$

A 2D similarity map S then can be formed by calculation on all pixels, to measure the similarity of the query x^q and key x^k in pixel-level.

Most existing works relied on the spatial distance between pixels to construct positive and negative pairs [27], which easily suffers from the erroneous outcomes for complex surgical scene. Instead, we pursue a more trustworthy way by leveraging our relatively precise pseudo label to navigate the process of forming pairs. It is based on the underlying assumption that embeddings of pixels belonging to the same class should be closer than those from different classes. Concretely, we perform the same augmentation on pseudo labels, and then couple $\{f_i^q, \hat{y}_i^q\}$ for pixel i in query image and $\{f_j^k, \hat{y}_j^k\}$ for pixel j in key image. For each key image, we define two 2D label selection masks \mathcal{M}^p and \mathcal{M}^n respectively for positives and negatives. Both of them are with a binary variable $\mathcal{M}^p, \mathcal{M}^n \subseteq \{0, 1\}^{HW \times HW}$, and value at ij is determined by the pseudo label:

$$\mathcal{M}_{ij}^p = \mathbb{1}[\hat{y}_i^q = \hat{y}_j^k], \quad \mathcal{M}_{ij}^n = 1 - \mathcal{M}_{ij}^p. \quad (2)$$

For the query pixel q_i , a key frame can provide both positive and negative pixel embeddings. If pseudo semantic labels \hat{y}_i^q and \hat{y}_j^k belong to the same class, Eq. 2 gives $\mathcal{M}_{ij}^p = 1$ to categorize k_j as the positive embeddings, otherwise, they are regarded as negative embeddings (cf. Fig. 3). With the guidance of label selection masks, we divide the similarity for query pixel q_i into the positive and negative portions

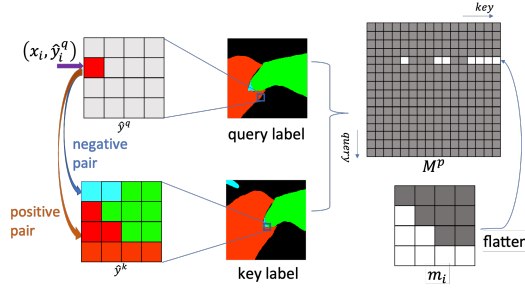


Fig. 3. A query pixel i forms positive pairs with pixels from key view having the same labels. Aligned with label \hat{y}^k , we get a positive map m_i of pixel i with label \hat{y}^q . Flatten and stack all maps of pixels in \hat{y}^q , we get a mask with the same size as similarity map.

through the element-wise production between the masks and similarity map:

$$S_i^p = \frac{1}{|\mathcal{P}_i|} \sum_{j \in \mathcal{P}_i} S_{ij} \odot \mathcal{M}_{ij}^p, \quad S_i^n = \frac{1}{|\mathcal{N}_i|} \sum_{j \in \mathcal{N}_i} S_{ij} \odot \mathcal{M}_{ij}^n, \quad (3)$$

where \mathcal{P}_i and \mathcal{N}_i are pixel embedding collections of positive ($\mathcal{M}_{ij}^p = 1$) and negative ($\mathcal{M}_{ij}^n = 1$) samples from the key image. Our pseudo label guided contrastive objective is then designed to maximize the masked positive similarities while minimize the masked negative ones (shown by the overall variant in Eq. 6).

C. Cross-video Contrast for Global Regularization

Many literatures demonstrate that contrastive learning can benefit from more positive and negative samples by creating more views [23], [31], which recently have been proved by an expansion and separation theory [32]. Apart from different views of a single frame created by the artificial augmentation (Sec. II-B), robotic surgical videos can inherently provide natural and more aggressive augmentations to construct more positives and negatives. However, utilizing temporal information for pair construction in pixel-level is difficult, as correspondence between pixels of different frames is unknown due to motion. Thanks to our pseudo-label guided strategy, where such correspondence can be more easily located, we can extend our contrastive learning from image-wise to video-wise by selecting pairs from different video frames. We present a hierarchically four-level selection strategy for our cross-video contrast learning, which can regularize model by considering global semantic knowledge of the whole dataset.

As shown in Fig. 2, conventional image-level set and view-level set contain the original image and its different perturbations (Sec. II-B). We first grow the pair hierarchy with the shot-level, aiming to increase the positives by borrowing the adjacent frames. Note that such adjacent frames are chosen from the same shot, instead of being simply selected from the same video. As in robotic surgery, visual content generally keeps consistent within a complete action, while shows a large variation when action transaction or some unexpected events happen. A surgical video therefore is presented as a set of several shots, where frames within each show high similarity. With the proceeding of video flow, intensity histogram changes slightly within the same

shot and changes severely when the video moves to next shot. In this regard, for the query image x from video V , we first exploit intensity histogram to partition V to several shots by detecting the severe change with a threshold. We then randomly sample N_a frames from the same shot as x , and couple them with pseudo labels (x^{ka}, \hat{y}^{ka}) followed by the same augmentation to generate the key views. It is then passed through momentum encoder to generate the key embeddings. We then expand the pair hierarchy to video-level, to leverage frames from other videos to increase negatives. Specifically, we randomly sample frames from other videos in video pool, resulting in N_v frame and pseudo label pairs (x^{kv}, \hat{y}^{kv}) . They go through same procedures, i.e., augmentation, feature extraction from momentum encoder, to mainly enrich negative key embeddings.

To this end, for the query pixel i , we also use Eq. 2 on more key pixels (with \hat{y}_j^{ka} and \hat{y}_j^{kv}) to increase the numbers of pseudo label selection masks to $N = N_a + N_v + N_c$, where N_c is the number of different views generated from the current frame. The masked positive and negative similarities in Eq. 3 can be augmented with updated \mathcal{P}_i and \mathcal{N}_i :

$$S_i^p = \frac{1}{|\mathcal{P}_i|} \sum_{j \in \mathcal{P}_i} S_{ij} \odot \mathcal{M}_{ij}^p; \quad (4)$$

$$S_i^n = \sum_{id=1}^N \frac{1}{|\mathcal{N}_i^{id}|} \sum_{j \in \mathcal{N}_i^{id}} S_{ij} \odot \mathcal{M}_{ij}^n, \quad \mathcal{N}_i^{id} \subset \mathcal{N}_i. \quad (5)$$

Here, the updated \mathcal{P}_i contains the three subsets, which respectively consist of the positive pixel embeddings provided by adjacent frames f_j^{ka} , frames from other videos f_j^{kv} , and the current frame with different augmentation f_j^{kc} . \mathcal{N}_i is augmented in the same way. For different query pixels, the number of positive/negative pairs can be largely different. Thus we use average value of similarities instead of summation value to make value of S_i^p and S_i^n stable. Note that we only average negative similarities in frame-level, with \mathcal{N}_i^{id} denoting the set of key pixels from one frame. Compared with the positive one that is further averaged all pixels cross frames, this strategy can enlarge the value of negative proportion to benefit the contrastive learning.

We devise a new contrastive objective to maximize positive similarities while minimize negative ones:

$$\mathcal{L} = -\frac{1}{k} \sum_{i=1}^k \log \frac{\exp(S_i^p)}{\exp(S_i^p) + \exp(S_i^n)}. \quad (6)$$

Note that in the learning process, only parameters of regular encoder θ are updated online via back propagation, while the momentum one θ^m to calculate the key are updated slowly by exponential moving average (EMA) [33]: $\theta^m \leftarrow m\theta^m + (1 - m)\theta$, where m is a momentum coefficient. Therefore, they provide relatively stable learning targets for the regular encoder to query. By making full use of similarities among the pixels, our contrastive learning can better shape the pixel embedding space. The well-structured space enables the model to only use limited annotations to achieve accurate segmentation.

TABLE I
RESULTS OF DIFFERENT METHODS ON ENDOVIS18 DATASET FOR SCENE SEGMENTATION.

Methods	Frames used		Overall	Sequence1	Sequence2	Sequence3	Sequence4
	Labeled Ratio	Unlabeled Ratio	mIoU(%)	mIoU(%)	mIoU(%)	mIoU(%)	mIoU(%)
DeepLabV3 (baseline) [34]	100%	0	58.48±0.43	63.86±0.59	54.98±0.98	80.81±0.23	34.25±1.26
DeepLabV3 (baseline) [34]	5.4%	94.6%	53.72±0.60	55.78±0.45	51.45±0.67	75.39±0.46	32.28±0.85
DMT [19]	5.4%	94.6%	53.70±0.16	56.23±0.20	50.78±0.16	74.42±0.27	33.37±0.51
PixPro [27]	5.4%	94.6%	55.47±1.08	58.66±1.45	52.26±1.23	78.42±0.76	32.50±2.31
UA-MT [22]	5.4%	94.6%	56.15±0.38	56.65±1.13	52.73±0.84	78.97±0.60	36.23±0.99
PGV-CL(Ours)	5.4%	94.6%	57.83±0.23	59.78±0.50	53.37±0.60	80.66±0.15	37.50±1.89
DeepLabV3 (baseline) [34]	10.1%	89.9%	56.76±0.30	61.07±0.38	52.69±0.19	78.99±0.15	34.27±1.17
DMT [19]	10.1%	89.9%	56.34±0.11	60.44±0.24	52.30±0.13	79.43±0.26	33.14±0.24
PixPro [27]	10.1%	89.9%	57.38±0.42	61.90±1.92	54.66±0.85	80.83±0.49	32.13±1.45
UA-MT [22]	10.1%	89.9%	57.21±0.63	58.02±0.56	55.06±0.48	79.87±0.85	35.86±1.13
PGV-CL(Ours)	10.1%	89.9%	58.59±0.14	62.70±0.58	54.53±0.87	81.32±0.57	35.81±1.68

TABLE II
RESULTS OF DIFFERENT METHODS ON CADIS DATASET FOR SCENE SEGMENTATION.

Methods	Frames used		Validation set			Test set		
	Labeled	Unlabeled	mIoU(%)	PA(%)	PAC(%)	mIoU(%)	PA(%)	PAC(%)
DeepLabV3 [34]	100%	0	86.12±0.17	94.28±0.05	92.38±0.17	82.47±0.07	93.29±0.04	88.72±0.13
DeepLabV3 [34]	1.9%	98.1%	78.99±0.15	92.05±0.08	86.13±0.21	75.50±0.17	91.88±0.07	83.11±0.07
DMT [19]	1.9%	98.1%	80.81±0.18	92.85±0.16	87.97±0.10	78.67±0.27	92.75±0.22	87.40±0.38
PixPro [27]	1.9%	98.1%	77.60±1.10	92.92±0.13	84.00±1.13	74.38±0.04	92.44±0.15	81.49±0.12
UA-MT [22]	1.9%	98.1%	77.45±0.16	92.54±0.18	84.31±0.40	76.02±0.84	92.08±0.23	83.46±0.83
PGV-CL(Ours)	1.9%	98.1%	81.57±0.48	93.82±0.08	87.88±0.37	78.81±0.07	93.13±0.06	85.73±0.00
DeepLabV3 [34]	2.3%	97.7%	80.76±0.09	92.70±0.04	87.73±0.06	79.15±0.08	92.54±0.04	86.29±0.11
DMT [19]	2.3%	97.7%	81.12±0.11	93.15±0.05	87.90±0.21	79.58±0.13	92.85±0.08	87.55±0.29
PixPro [27]	2.3%	97.7%	80.72±1.14	93.26±0.03	87.25±1.35	79.14±0.39	92.87±0.10	86.05±0.64
UA-MT [22]	2.3%	97.7%	81.97±0.13	93.09±0.17	88.80±0.51	79.24±0.28	92.64±0.10	86.11±0.38
PGV-CL(Ours)	2.3%	97.7%	83.75±0.85	94.04±0.23	90.09±0.73	81.49±0.34	93.48±0.14	87.85±0.37

III. EXPERIMENTS

We first introduce two datasets and metrics used to evaluate our method. And then we report implementation details of our method. Further, we compare our methods with other semi-supervised segmentation methods. At last, we ablate two important factors that influence our method.

A. Datasets and Evaluation Metrics

EndoVis18: The EndoVis18 is a public challenge dataset from 2018 MICCAI Robotic Scene Segmentation challenge [4]. This dataset consists of 19 sequences among which 15 sequences are for training and 4 sequences for testing. All sequences are recorded on da Vinci X or Xi system during porcine training procedure. Each frame is of a high resolution of 1280×1024 . The dataset parses the scene into 12 classes, including different robotic instruments and anatomies.

CaDIS: The CaDIS dataset is a public benchmark focusing on the eyes of patients during the cataract surgery [9]. It consists of 25 videos, with 19 videos as training set, 3 videos as validation set and 3 videos as test set. All videos are recorded using a 180I camera mounted on an OPMI Lumera T microscope and each frame has a high resolution of 960×540 . The scene is divided into 8 classes with 4 classes for anatomical tissues, 1 class for all instruments, and 3 classes for all other objects appearing in the scene.

For fair comparison, we follow EndoVis18 challenge to use mean intersection-over-union (mIoU) as metrics to evaluate methods. Overall and results on four test sequences are reported. Also following CaDIS benchmark, we employ

mIoU, Pixel Accuracy (PA), Pixel Accuracy per Class (PAC) as metrics and report results on both validation and test set.

B. Implementation Details

We use DeepLabV3 [34] as our segmentation model and ResNet-50 [35] pre-trained on ImageNet [36] as encoder. We employ a three-stage training strategy to train our model \mathcal{F}^s , i.e., pre-training, contrastive learning, and fine-tuning. We first train the segmentation model using the labeled data \mathcal{D}_L . The pre-trained model generates pseudo labels for unlabeled frames and serves as model initialization for contrastive learning. Next, we perform the proposed contrastive learning paradigm to extract the knowledge by adding unlabeled data $\mathcal{D}_L \cup \hat{\mathcal{D}}_U$ (pseudo labels replaced by ground truths for labeled data). We take all layers of \mathcal{F}^s except the last two layers (used as classifier) as backbone, and develop a projector consisting of two 1×1 convolutional layers to reduce the channels. Finally, we reuse the labeled data \mathcal{D}_L to fine-tune our segmentation model \mathcal{F}^s . We exploited Online Hard Example Mining (OHEM) [37] as loss objective in this stage.

Our framework is implemented in PyTorch with two NVIDIA Titan Xp GPUs. All video frames are resized to the resolution of 480×480 in the pre-training and fine-tuning stages. We deploy SGD optimizer [38] with a poly learning rate scheduler and use a base learning rate of $1e-3$ for optimize supervised loss in these two stages. Batch size is 8. In contrastive learning, we randomly crop a patch (resolution ranging from 144×144 to 336×336) from a frame to create more aggressive augmentation and resize it to 480×480 to match the resolution used in fine-tuning. We use

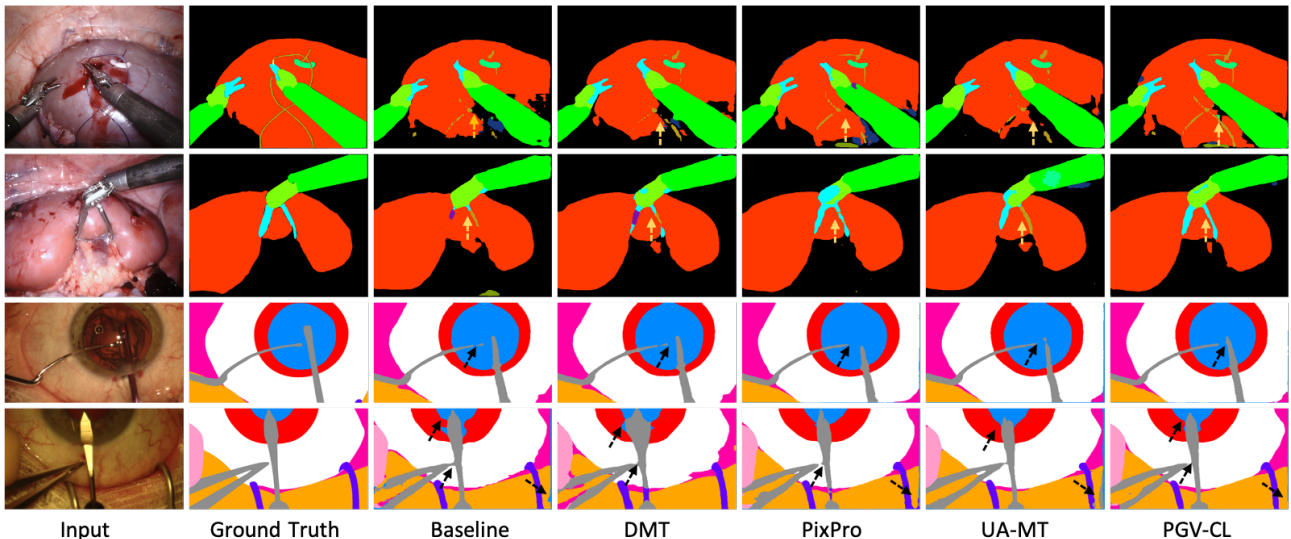


Fig. 4. Qualitative comparison on 10.1% labeled EndoVis18 and 2.3% labeled CaDIS datasets. More results can be found in supplementary video.



Fig. 5. Pixel embeddings from baseline w/o contrast (left) and ours w/ contrast (right) on EndoVis18. Different colors represent different classes.

LARS optimizer [39] with a cosine learning rate scheduler and set a base to 1. Batch size is 4 and weight decay is $1e-5$. Optimizing contrastive loss takes around 7 hours for EndoVis18 and 11 hours for CaDIS with 140 epochs.

C. Comparison with State-of-the-art Methods

We implement several state-of-the-art semi-supervised methods for comparison, including *DMT* [19]: a pseudo-labeling based method, which deploy two differently initialized models to generate pseudo labels for mutual training; *PixPro* [27]: a contrastive learning method, which form positive and negative pairs based on the spatial distance; *UA-MT* [22]: a consistency regularization method based on the mean teacher, which jointly train the model by segmentation loss and consistency loss. For fair comparison, all these use the same segmentation model as our method (i.e. DeepLabV3 with ResNet-50). And we implement these methods based on the officially released code, utilize the pre-trained model from ImageNet, and tune some important hyper-parameters on our datasets to get better results. Note that for Pixpro, we only replace the contrastive learning stage with other stages remaining the same as our method. Additionally, we provide a *Baseline* model, that is trained only using the labeled data. All the experiments are repeated 3 times to avoid the case of coincidence and their average results are reported.

Our experiments are conducted on very limited annotation settings, i.e., 5.4% and 10.1% frames being labeled with

intervals as 20 and 10 on EndoVis18. Given CaDIS is collected at a higher frequency than EndoVis18 (30 fps v.s. 1 fps), only 1.9% and 2.3% frames are labeled with intervals of 60 and 50. The segmentation results on the two datasets are summarized in Table I and Table II. We found that by effectively leveraging the unlabeled data, our method can greatly improve the performance compared with the baseline model, i.e., increasing mIoU ranging from 1.83% to 4.11% on the four settings. Among the semi-supervised methods, regarding pseudo label as ground truth to explicitly calculate the loss for model penalization, DMT even degrades results compared with baseline in some extreme annotation settings. Instead, our method leverages the pseudo label to guide the contrastive learning, largely boosting the segmentation performance. Meanwhile, compared with Pixpro which relies on the pixel distance for pair construction, the goal of both methods is to pull (push) representations of pixel pair belonging to the same (different) class. Our method achieves superior results, indicating that it can provide more reliable and global model regularization by using pseudo labels to navigate the contrast of pixels across videos. Additionally, our method consistently outperforms the method that performs the consistency regularization on the model predictions (UA-MT), across all the four settings on two datasets. The improvement degree is larger as the amount of annotations decrease. We gain the maximum benefits in the severest condition (1.9% labeling on CaDIS), with 4.12% and 2.79% mIoU increase over UA-MT on validation and test set. Notably, our method trained with only partly labeled data can even surpass the fully supervised model in some case (10.1% labeling on EndoVis18).

We show the visual comparison in Fig. 4. Our method can detect small objects such as thread in row 1 and instrument tips in row 2, and also achieve more complete prediction for large one. Fig. 5 visualizes the pixel embeddings extracted from baseline and our model with t-SNE [40]. As pixel-wise features are enormous for all test data, we select five typical

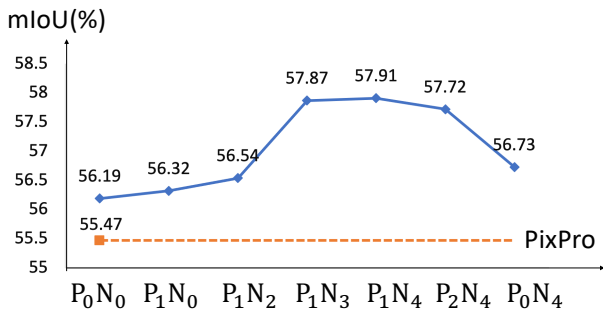


Fig. 6. Ablation study on different amounts of positive and negative pairs.

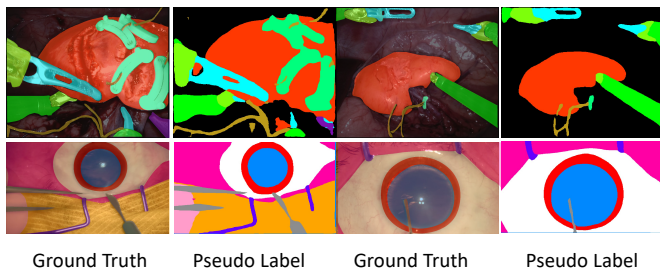


Fig. 7. Visualization of generated pseudo labels.

frames to cover all classes. We can see that our contrastive learning enables a more separable feature space. Some pixels in the same class although may be divided into two clusters given that they’re from different objects and show different appearance, they are more compact for easy distinguishing.

D. Ablation Studies

1) *Positive and negative pair construction*: The pair construction is a key factor in contrastive learning. We analyze its effect on the segmentation results under different qualities, i.e., formed based on spatial distance (Pixpro) and formed guided by pseudo labels (Ours). We further study its effect with different quantities by varying the value of positive and negative pairs, resulting in six configurations. With each current frame as the query frame, P_iN_j means that the numbers of adjacent frames and frames from other videos which we utilize as key frames are i and j , respectively. All experiments are conducted on EndoVis18 dataset with 5.4% labeled frames. The results from a single experiment running for each setting are presented in Fig. 6.

We can see that when the query and key feature maps solely come from a current frame without leveraging the others (P_0N_0), our method increase 0.72% over the Pixpro, demonstrating that our pseudo label guided strategy promotes the precise on pair construction for better contrastive learning. We further visualize our generated pseudo labels in Fig. 7 for more intuitive explanation. We can see that they are of high quality and can largely overlap with the ground truths, therefore providing the accurate instruction for pair selection. Moreover, our pseudo label strategy enables to construct pairs by leveraging other frames, while Pixpro fails to take advantage of it. Comparing results of P_0N_4 , P_1N_4 we see that the adjacent frame mainly providing positive pairs can greatly help achieve the superior performance. When

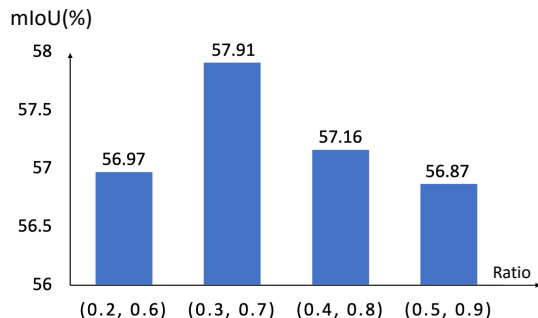


Fig. 8. Ablation study on patch crop size in data augmentation.

increasing the value of j to introduce more negative pairs (P_1N_2 , P_1N_3 , and P_1N_4), segmentation results gradually improve while show a slow trendy when it is larger than 3. The performance degrades with P_2N_4 , given that more positives need more negatives to optimize. But including too many negatives is unfeasible, as we do need to consider the practical computation resource for pair construction. In our work, we therefore choose one adjacent frame and four frames from other videos in pair construction.

2) *Crop size of patches*: We then analyze the patch crop size, an important augmentation hyperparameter in our contrastive learning. Specifically, we vary the minimal (*min*) and maximal (*max*) side length in the range of $(0, 1]$. The results of different (*min*, *max*) values on EndoVis18 dataset with 5.4% labeling are shown in Fig. 8. Overall, our method is not very sensitive to this parameter, achieving the stable mIoU around 57%. Analyzing in detail, we observe that the higher performance can be achieved when increasing *min* from 0.2 to 0.3. While when *min* > 0.3, the results starts decreasing. The underlying reason is that the crop size directly influences the overlapped area and the amount of formed positive pairs. Too scarce or redundant positive pairs may lead to the training difficulty in contrastive learning.

IV. CONCLUSIONS AND FUTURE WORK

In this work, we propose a pseudo-label guided cross-video pixel contrast method for label-efficient surgical scene segmentation. The proposed method addresses the scarcity of annotated frames by providing a novel approach to utilize unlabeled video frames. We generate relatively accurate pseudo labels by sampling labeled frames equidistantly and then use pseudo labels as guidance to conduct pixel-level contrastive learning. To further improve the performance, we construct pairs in contrastive learning from video-wise. Our method achieves promising results on two real-world datasets EndoVis18 and CaDIS, and greatly reduces the burden of annotation. In our future work, we shall explore how to solve class imbalance problem by introducing re-weighting and re-sampling strategies into contrastive learning. Moreover, we will investigate how to leverage the multi-modal resources, such as multi-view stereo images and depth information, to improve the performance. We will also investigate how to select frames as labelled ones based on active learning to further reduce labelling burden.

REFERENCES

- [1] J. H. Palep, "Robotic assisted minimally invasive surgery," *Journal of minimal access surgery*, vol. 5, no. 1, p. 1, 2009.
- [2] L. Maier-Hein, S. S. Vedula, S. Speidel, N. Navab, R. Kikinis, A. Park, M. Eisenmann, H. Feussner, G. Forestier, S. Giannarou *et al.*, "Surgical data science for next-generation interventions," *Nat. Biomed. Eng.*, vol. 1, no. 9, pp. 691–696, 2017.
- [3] B. Poursartip, M.-E. LeBel, R. V. Patel, M. D. Naish, and A. L. Trejos, "Analysis of energy-based metrics for laparoscopic skills assessment," *IEEE Transactions on Biomedical Engineering*, vol. 65, no. 7, pp. 1532–1542, 2018.
- [4] M. Allan, S. Kondo, S. Bodenstedt, S. Leger, R. Kadkhodamohammadi, I. Luengo, F. Fuentes, E. Flouty, A. Mohammed, M. Pedersen *et al.*, "2018 robotic scene segmentation challenge," *arXiv preprint arXiv:2001.11190*, 2020.
- [5] M. Allan, S. Ourselin, D. J. Hawkes, J. D. Kelly, and D. Stoyanov, "3-d pose estimation of articulated instruments in robotic minimally invasive surgery," *IEEE transactions on medical imaging*, vol. 37, no. 5, pp. 1204–1213, 2018.
- [6] X. Du, M. Allan, S. Bodenstedt, L. Maier-Hein, S. Speidel, A. Dore, and D. Stoyanov, "Patch-based adaptive weighting with segmentation and scale (pawss) for visual tracking in surgical video," *Medical image analysis*, vol. 57, pp. 120–135, 2019.
- [7] T. D. Nagy and T. Haidegger, "A dvrk-based framework for surgical subtask automation," *Acta Polytechnica Hungarica*, pp. 61–78, 2019.
- [8] X. Ren, S. Ahmad, L. Zhang, L. Xiang, D. Nie, F. Yang, Q. Wang, and D. Shen, "Task decomposition and synchronization for semantic biomedical image segmentation," *IEEE Transactions on Image Processing*, vol. 29, pp. 7497–7510, 2020.
- [9] M. Grammatikopoulou, E. Flouty, A. Kadkhodamohammadi, G. Quellec, A. Chow, J. Nehme, I. Luengo, and D. Stoyanov, "Cadis: Cataract dataset for surgical rgb-image segmentation," *Medical Image Analysis*, vol. 71, p. 102053, 2021.
- [10] B. Wang, L. Li, Y. Nakashima, R. Kawasaki, H. Nagahara, and Y. Yagi, "Noisy-lstm: Improving temporal awareness for video semantic segmentation," *IEEE Access*, vol. 9, pp. 46 810–46 820, 2021.
- [11] Y. Jin, Y. Yu, C. Chen, Z. Zhao, P.-A. Heng, and D. Stoyanov, "Exploring intra-and inter-video relation for surgical semantic scene segmentation," *IEEE Transactions on Medical Imaging*, 2022.
- [12] D.-H. Lee *et al.*, "Pseudo-label: The simple and efficient semi-supervised learning method for deep neural networks," in *Workshop on challenges in representation learning, ICML*, vol. 3, no. 2, 2013, p. 896.
- [13] A. Iscen, G. Toliás, Y. Avrithis, and O. Chum, "Label propagation for deep semi-supervised learning," in *Proceedings of the IEEE/CVF Conference on Computer Vision and Pattern Recognition*, 2019, pp. 5070–5079.
- [14] Y. Jin, K. Cheng, Q. Dou, and P.-A. Heng, "Incorporating temporal prior from motion flow for instrument segmentation in minimally invasive surgery video," in *International Conference on Medical Image Computing and Computer-Assisted Intervention*. Springer, 2019, pp. 440–448.
- [15] Z. Zhao, Y. Jin, X. Gao, Q. Dou, and P.-A. Heng, "Learning motion flows for semi-supervised instrument segmentation from robotic surgical video," in *International Conference on Medical Image Computing and Computer-Assisted Intervention*. Springer, 2020, pp. 679–689.
- [16] Y. Zou, Z. Yu, B. Kumar, and J. Wang, "Unsupervised domain adaptation for semantic segmentation via class-balanced self-training," in *Proceedings of the European conference on computer vision (ECCV)*, 2018, pp. 289–305.
- [17] W.-C. Hung, Y.-H. Tsai, Y.-T. Liou, Y.-Y. Lin, and M.-H. Yang, "Adversarial learning for semi-supervised semantic segmentation," *arXiv preprint arXiv:1802.07934*, 2018.
- [18] M. N. Rizve, K. Duarte, Y. S. Rawat, and M. Shah, "In defense of pseudo-labeling: An uncertainty-aware pseudo-label selection framework for semi-supervised learning," *arXiv preprint arXiv:2101.06329*, 2021.
- [19] Z. Feng, Q. Zhou, Q. Gu, X. Tan, G. Cheng, X. Lu, J. Shi, and L. Ma, "Dmt: Dynamic mutual training for semi-supervised learning," *arXiv preprint arXiv:2004.08514*, 2020.
- [20] G. French, S. Laine, T. Aila, M. Mackiewicz, and G. Finlayson, "Semi-supervised semantic segmentation needs strong, varied perturbations," *arXiv preprint arXiv:1906.01916*, 2019.
- [21] A. Tarvainen and H. Valpola, "Mean teachers are better role models: Weight-averaged consistency targets improve semi-supervised deep learning results," *arXiv preprint arXiv:1703.01780*, 2017.
- [22] L. Yu, S. Wang, X. Li, C.-W. Fu, and P.-A. Heng, "Uncertainty-aware self-ensembling model for semi-supervised 3d left atrium segmentation," in *International Conference on Medical Image Computing and Computer-Assisted Intervention*. Springer, 2019, pp. 605–613.
- [23] T. Chen, S. Kornblith, M. Norouzi, and G. Hinton, "A simple framework for contrastive learning of visual representations," in *International conference on machine learning*. PMLR, 2020, pp. 1597–1607.
- [24] X. Chen, H. Fan, R. Girshick, and K. He, "Improved baselines with momentum contrastive learning," *arXiv preprint arXiv:2003.04297*, 2020.
- [25] K. Chaitanya, E. Erdil, N. Karani, and E. Konukoglu, "Contrastive learning of global and local features for medical image segmentation with limited annotations," *arXiv preprint arXiv:2006.10511*, 2020.
- [26] X. Lai, Z. Tian, L. Jiang, S. Liu, H. Zhao, L. Wang, and J. Jia, "Semi-supervised semantic segmentation with directional context-aware consistency," in *Proceedings of the IEEE/CVF Conference on Computer Vision and Pattern Recognition*, 2021, pp. 1205–1214.
- [27] Z. Xie, Y. Lin, Z. Zhang, Y. Cao, S. Lin, and H. Hu, "Propagate yourself: Exploring pixel-level consistency for unsupervised visual representation learning," in *Proceedings of the IEEE/CVF Conference on Computer Vision and Pattern Recognition*, 2021, pp. 16 684–16 693.
- [28] X. Zhao, R. Vemulapalli, P. Mansfield, B. Gong, B. Green, L. Shapira, and Y. Wu, "Contrastive learning for label-efficient semantic segmentation," *arXiv preprint arXiv:2012.06985*, 2020.
- [29] Y. Zhou, H. Xu, W. Zhang, B. Gao, and P.-A. Heng, "C3-semiseg: Contrastive semi-supervised segmentation via cross-set learning and dynamic class-balancing," in *Proceedings of the IEEE/CVF International Conference on Computer Vision*, 2021, pp. 7036–7045.
- [30] W. Wang, T. Zhou, F. Yu, J. Dai, E. Konukoglu, and L. Van Gool, "Exploring cross-image pixel contrast for semantic segmentation," in *Proceedings of the IEEE/CVF International Conference on Computer Vision*, 2021, pp. 7303–7313.
- [31] K. He, H. Fan, Y. Wu, S. Xie, and R. Girshick, "Momentum contrast for unsupervised visual representation learning," in *Proceedings of the IEEE/CVF Conference on Computer Vision and Pattern Recognition*, 2020, pp. 9729–9738.
- [32] C. Wei, K. Shen, Y. Chen, and T. Ma, "Theoretical analysis of self-training with deep networks on unlabeled data," *arXiv preprint arXiv:2010.03622*, 2020.
- [33] J. S. Hunter, "The exponentially weighted moving average," *Journal of quality technology*, vol. 18, no. 4, pp. 203–210, 1986.
- [34] L.-C. Chen, G. Papandreou, F. Schroff, and H. Adam, "Rethinking atrous convolution for semantic image segmentation," *arXiv preprint arXiv:1706.05587*, 2017.
- [35] K. He, X. Zhang, S. Ren, and J. Sun, "Deep residual learning for image recognition," in *Proceedings of the IEEE conference on computer vision and pattern recognition*, 2016, pp. 770–778.
- [36] J. Deng, W. Dong, R. Socher, L.-J. Li, K. Li, and L. Fei-Fei, "Imagenet: A large-scale hierarchical image database," in *2009 IEEE conference on computer vision and pattern recognition*. Ieee, 2009, pp. 248–255.
- [37] A. Shrivastava, A. Gupta, and R. Girshick, "Training region-based object detectors with online hard example mining," in *Proceedings of the IEEE conference on computer vision and pattern recognition*, 2016, pp. 761–769.
- [38] S. Ruder, "An overview of gradient descent optimization algorithms," *arXiv preprint arXiv:1609.04747*, 2016.
- [39] Y. You, I. Gitman, and B. Ginsburg, "Large batch training of convolutional networks," *arXiv preprint arXiv:1708.03888*, 2017.
- [40] L. Van der Maaten and G. Hinton, "Visualizing data using t-sne," *Journal of machine learning research*, vol. 9, no. 11, 2008.